Injury-induced Semaphorin6C/PlexinA2 signaling drives remote neuronal apoptosis and functional impairment in the adult CNS

Maria Teresa Viscomi

mariateresa.viscomi@unicatt.it

Università Cattolica del Sacro Cuore https://orcid.org/0000-0002-9096-4967

Sofia Nutarelli

Università Cattolica del S. Cuore

Francesca Rech

Università Cattolica del S. Cuore

Viviana Greco

Università Cattolica del Sacro Cuore

Anna Percio

Università Cattolica del S. Cuore

Andrea Urbani

Università Cattolica del S. Cuore

Luca Tamagnone

Università Cattolica del Sacro Cuore https://orcid.org/0000-0002-2884-7946

Daniela Palacios

CNR, Rome, Italy

Article

Keywords: axonal injury, secondary neurodegeneration, functional recovery, neuroinflammation, microglia, axotomy

Posted Date: July 31st, 2026

DOI: https://doi.org/10.21203/rs.3.rs-10267729/v1

Additional Declarations: (Not answered)

Abstract

Axonal degeneration is a major driver of disability and disease progression in several central nervous system (CNS) disorders. After injury, neurodegeneration may extend beyond the primary lesion to anatomically and functionally connected neuronal populations, contributing to secondary damage and impaired recovery. Semaphorins are developmental axon guidance molecules that may be reactivated in the adult CNS after injury. Here, we investigated whether semaphorin 6C (Sema6C), a poorly characterized semaphorin, contributes to remote neuronal degeneration after axonal damage.

We used a mouse model of hemicerebellectomy (HCb), a focal CNS injury paradigm, in which unilateral removal of the cerebellar hemisphere induces axotomy and deafferentation of precerebellar neurons, particularly those of pontine nuclei. This model enables the study of remote secondary degeneration in neuronal populations anatomically connected to the primary lesion site. To define the role of Sema6C and its receptor Plexin A2 in this process, we integrated proteomic profiling, *in situ* hybridization, genetic silencing, recombinant protein administration, morphological analyses, and behavioral assessments.

Sema6C was selectively upregulated in pontine neurons after HCb, in association with inflammatory pathway activation and JNK-dependent apoptotic signaling. *In vivo* Sema6C silencing reduced JNK phosphorylation and caspase-3 activation, preserved neuronal survival, and improved functional recovery. Conversely, intracerebroventricular administration of recombinant Sema6C exacerbated remote neuronal death, worsened neurological outcomes, and amplified apoptotic and neuroinflammatory responses, including increased CD68 expression and microglial remodeling. Mechanistically, Plexin A2 was identified as a Sema6C-interacting receptor upregulated in injured pontine neurons. Plexin A2 knockdown reproduced the neuroprotective effects of Sema6C silencing both *in vitro* and *in vivo*.

These findings identify Sema6C/Plexin A2 signaling as an injury-induced pathway that links axonal damage to maladaptive neuroinflammation, JNK activation, and secondary neuronal loss. Targeting this pathway may represent a promising strategy to limit remote neurodegeneration and improve recovery after CNS injury.

Introduction

Neurons in the adult central nervous system (CNS) rely on the extraordinary length and integrity of their axons to sustain connectivity and function[1]. Yet, this same architecture renders them acutely vulnerable: even localized axonal injury can initiate a cascade of degenerative events that extend far beyond the lesion site[2, 3]. In many neurological conditions, axonal damage precedes and predicts neuronal loss, often culminating in the delayed degeneration of the soma through a process known as “dying-back”[4–6]. Despite its central role in disease progression, the molecular mechanism by which distal axonal injury is communicated to the cell body—and translated into either survival or death—remains incompletely understood.

Following axonal injury, axotomized neurons activate a complex and dynamic signaling network that integrates stress responses, metabolic alterations, and intracellular transport mechanisms[7]. Pathways involving mitochondrial dysfunction, oxidative stress, autophagy, and receptor-mediated signaling have all been implicated in shaping neuronal fate[8–11]. Importantly, these processes unfold over time, revealing a critical window during which degenerative trajectories may still be reversed or attenuated[3]. A key unresolved question is how these diverse signals are coordinated, and whether common upstream regulators exist that tip the balance between repair and degeneration.

A growing body of evidence indicates that axonal injury in the adult CNS reactivates molecular programs typically confined to development[12–15]. During embryogenesis, neuronal wiring is orchestrated by highly conserved guidance cues that direct axonal growth, navigation, and target selection. Among these, semaphorins play a central role in sculpting neural circuits[16–18]. While largely quiescent in the mature nervous system, semaphorin signaling can be robustly re-induced under conditions of injury, inflammation, or cellular stress[19, 20]. This reactivation suggests that adult neurons may, in effect, revert to a development-like signaling state associated with axonal retraction, growth cone collapse, or neuronal apoptosis [21–25].

Within this framework, semaphorins have increasingly been implicated as key modulators of neurodegenerative processes[26–28]. Secreted class 3 semaphorins, such as Sema3A, and transmembrane members like Sema4D have been linked to neuronal loss, synaptic dysfunction, and neuroinflammation across multiple disease contexts[29–35]. The size and diversity of the semaphorin family, together with the roles of many of its members in the adult CNS, remain largely unexplored. Here we focused our attention on a relatively understudied transmembrane family member, Semaphorin 6C (Sema6C), that we found upregulated in axotomized neurons. Sema6C is expressed in both neurons and peripheral target tissues, where it contributes to axonal guidance and synapse formation during development[36]. However, its role in the adult nervous systems is currently unknown. Notably, emerging evidence from cancer biology reveals a striking functional duality: Sema6C can suppress cell proliferation through inhibition of the AKT/GSK3/β-catenin/Cyclin D1 axis[37], yet in other contexts it promotes survival and growth via distinct signaling pathways[38]. These apparently opposing effects suggest that Sema6C may exert bidirectional and context-specific functions also in the nervous system, potentially influencing neuronal vulnerability or resilience after injury.

Understanding whether Sema6C promotes neuronal survival, degeneration, or adaptive remodeling following axonal injury could therefore provide important insight into the mechanisms of axon-to-soma communication and remote neuronal responses after trauma. Here, by using an experimental model of CNS axonal injury, namely hemicerebellectomy (HCb), we demonstrated that the damage concurrently induces Sema6C up-regulation and neuronal apoptotic cell death in the pontine neurons, which suggested a key role of the semaphorin in conditioning the fate of axotomized neurons. Genetic modulation of Sema6C expression indeed significantly limited neuronal cell death and improved functional recovery, whereas intracerebroventricular administration of recombinant Sema6C exacerbated

neuronal loss, worsening the functional outcome. Our findings identify Sema6C as a key mediator of remote degeneration after HCb and demonstrate that its deleterious effects are mediated through Plexin A2. This highlights the Sema6C/Plexin A2 as a potential therapeutic target to attenuate neuronal death and improve functional recovery after focal CNS injury.

Methods

Animals, surgery and neurological assessment

All animal procedures were performed in accordance with the Animal Care and Use Committee and the Guidelines of The European Union Council (2010/6106/UE) and approved by the Italian Ministry of Health (Prot. Number: #436/2024-PR). Cerebellar lesions were attained by performing a right HCb, as described previously[10]. Intracerebroventricular (i.c.v.) injection of 200ng/ml Recombinant Mouse Semaphorin 6C Protein, CF (R&D Systems, # 2108-S6) was performed. Pontine nuclei injection of 10uM siRNA for Sema6c (Sigma, SASI_MM02_0032–0497), Plxna2 (Sigma, SASI_MM01_0005-3042) and scramble (Sigma, SIC002-10nmol) were performed by injecting at the following coordinates: AP-4.2, DV 5.5 and ML -0.5. Neurological severity score (NSS) was assessed 1 and 4 days after damage by an investigator blinded to the experimental groups, as previously described[39].

Sample preparation for mass spectrometry analysis

Each protein sample was subjected to protein digestion following the Filter-Aided Sample Preparation (FASP) protocol as described[40]. Briefly, 50 µg of proteins resulting from each condition were reduced (DTT 8 mM in 8 M urea buffer and 100 mM Trizma Base), alkylated (IAA 50 mM in 8 M urea buffer and 100 mM Trizma Base) and then digested with trypsin (final trypsin concentration of 0.01 µg/µL) overnight at 37°C on Microcon Centrifugal Filter Devices (Merck Millipore Ltd., Cork, Ireland).

LC-MS/MS analysis

Liquid chromatography-mass spectrometry (LC-MS) analysis were performed by an UltiMate 3000 RSLC nano – HPLC System (Thermo Fisher Scientific, Waltham, MA, USA) coupled with a high-resolution Orbitrap Fusion Lumos Tribrid Mass Spectrometer (Thermo Fisher Scientific) equipped with a Nanospray Flex source (Thermo Fisher Scientific). Specifically, Tryptic peptides (0. 5 µg) from each digested sample were loaded into a PepMap RSLC C18 column (2 µm, 100 Å, 50µm × 15 Cm; Thermo Scientific.) maintained at 40°C and then separated by a 155-minute reversed-phase gradient at 0,3 µL/min flow rate. Eluent A consisted of an aqueous solution of 0.1% FA, while eluent B was ACN with 0.1% FA. The gradient program was set as follows: 0% B and 100% A (min 0-110), 20% B and 80% A (min 110–120), 40% B and 60% A (min 120–125), 90% B and 10% A (min 125–145), 3% B and 97% A (min 145–155).The separated peptides were analysed using an Orbitrap Fusion Lumos Tribrid mass spectrometer operating in positive ionization mode (2100 V), with fragmentation performed in a Higher-energy Collision

Dissociation (HCD) cell and data acquired in Data-Dependent Acquisition (DDA) mode. The MS scan parameters were set as follows: Orbitrap resolution, 120,000; scan range (m/z), 350–1600. The MS/MS scan parameters were: Orbitrap resolution, 15,000. All samples were analysed in analytical triplicates.

Protein identification and label free quantification

MS raw data were analysed with the software Proteome Discoverer (v. 2.4.1). The qualitative identification of proteins was obtained by searching all reviewed proteins (Swiss-Prot) within the UniProt Mus Musculus reference proteome (ID: UP000000589, Taxon ID:10090). The search parameters used were set as follows: parent mass error tolerance automatic 10.0 ppm; fragment mass error tolerance 0.02 Da; minimum of 3 fragment ions matched per protein; minimum of 3 peptides matched per protein; maximum 2 missed cleavages. Carbamidomethylation of cysteines was set as a static modification, while oxidation of methionines, methionine loss, acetylation of lysines and N-terminal acetylation, were included as dynamic modifications. A false discovery rate (FDR) threshold of less than 1% was applied to the identification algorithm. The expression analysis was performed considering the technical replicates available for each experimental condition based on the hypothesis that each group was an independent variable. The list of differentially expressed proteins was screened according to a fold change of regulation higher than 30%. Only modulated proteins with $p < 0.05$ were considered significant. Over-representation analysis was carried out using the R package ClusterProfiler[41].

RNA extraction, retrotranscription and qPCR

RNA was extracted from PN using Total RNA Purification Kit from Norgen Biotek (Canada) according to the manufacturer's instructions. Then, 1 µg of total RNA was used for RT reaction by using the PrimeScript™ RT reagent Kit (Perfect Real Time) (Takara, Cat. #RR037A). The following RT program was used: 37°C for 15 min and 85°C for 5 s. The expression of the different primers was assessed by quantitative qPCR using TB Green® Premix Ex Taq™ II (Tli RNaseH Plus), Bulk (Takara, Cat. #RR820L) as a fluorescent dye to monitor cDNA amplification. The following PCR program was used: 50°C for 2 min, 40 cycles at 95°C for 15 s and 60°C for 60 s, melt curve 95°C for 15 s, 60°C for 60 s and 95°C for 30 s. The primers used were listed in Supplemental Table 1. GAPDH was used as a housekeeping gene for quantity normalization. Fold change was determined by using the ΔΔC(t) method.

Multiplex RNAscope™ and confocal analysis

Mice were anesthetized with Rompun (xylazine, 20 mg/ml, 0.5 ml/kg Bayer, Milan, Italy) and Zoletil (tiletamine and zolazepam, 100 mg/ml, 0.5 ml/kg; Virbac, Milan, Italy) and perfused transcranially with 25 ml of saline followed by 25 ml of 4% paraformaldehyde in a phosphate buffer (PB; 0.1 M; pH 0.4) under deep anesthesia. Each brain was removed immediately, post-fixed in the same fixative for 24 h and, after three washes in PB, transferred to 30% sucrose in PB solution at 4°C until they sinked. For RNAscope™ brains were cut into four series of 20µm-thick coronal sections by means of a freezing

microtome and were collected in PB. RNAscope™ (Advanced Cell Diagnostic, USA) was performed according to the manufacturer's protocol. Sections were dehydrated and post fixated according to the protocol, then peroxidase was applied, and antigen retrieval was performed. The following RNA probe was used: Mm-Sema6C-C1 (#1198611-C1) for Sema6C. Then the amplification cascade was performed as stated in the manufacturer's protocol and detected by using TSA-Vivid™ fluorophores 570. Before RNAscope processing, sections were incubated with primary antibodies including rabbit anti-NeuN antibody (1:400, cod. #24307S; CST), rabbit anti-GFAP (1:600, #AB9598, Merck), goat anti-Iba1 (1:600, #NB100-1028, Novus) and rabbit anti-Olig2 (1:200, cod. #ab109186, Abcam). After the RNAscope protocol, sections were incubated for 1h at RT with secondary antibodies including Alexa Fluor 488 donkey anti-rabbit IgG or Alexa Fluor 488 donkey anti-goat (1:200, Thermo Fisher). Sections were 4,6-diamidino-2-phenylindole (DAPI) counterstained (1:1000, Sigma). Sections were air-dried and coverslipped with GEL/MOUNT (Biomeda, Foster City, CA, USA). Sections were examined under a confocal laser-scanning microscope Nikon APM1 equipped with four laser lines: violet diode emitting at 405 nm (for DAPI), argon emitting at 488 nm, and helium/neon emitting at 543 nm and 633. The optical density (O.D.) for both mRNA and proteins were performed by densitometric analyses manually outlining individual cells and measuring cell-associated fluorescence intensity with the ImageJ software (http://rsb.info.nih.gov/ij/). The Mean/Area ratio defines mean fluorescence of individual cells normalized to total cellular surface. Quantification was done on 50 cells per mice.

Stereological analysis

To assess the extent of neuronal loss in the contralateral PN following HCb, stereological cells count following Nissl staining was performed. By using the Stereo Investigator System (MicroBrightField Europe e.K., Magdeburg, Germany) a three-dimensional optical fractionator counting probe (x, y, z dimension of 50 × 50 × 10µm, respectively) was applied to obtain unbiased estimates of total cells according to published procedures[42]. The PN was outlined using the 4x objective and the 100x oil immersion objective was used for marking the neuronal cells. The total number of neurons was estimated according to the formula: N1/4SQ=ssf1 = asf1=tsf, where SQ represents the total number of neurons counted in all optically sampled fields of the PN, ssf is the section sampling fraction, asf is the area sampling fraction, and tsf is the thickness sampling fraction. For each animal, 7 sections covering the rostro-caudal extension of the PN were counted. Data collecting for stereology was done by an experimenter blind to the group analyzed.

Tissue extraction and immunoblotting

The brains were immediately dissected in fresh PBS and the contralateral PN respect to the lesion was collected. Once isolated, the PNs were homogenized in RIPA buffer (Tris HCl pH = 7.4 50mM, NaCl 150mM, EDTA 1mM, MgCl2 5mM, Sodium deoxycholate 0.25%, TritonX100 1%, SDS 0.1%) with DTT (PanReac AppliChem, #A2948,005) and protease inhibitor cocktail (Sigma, #P8340), incubated on ice for 20 min and centrifuged at 13,000 × g for 20 min. The total protein content of the resulting supernatant

was determined. To assess the release of cytochrome-c in the cytosol we separated mitochondrial and cytosolic fraction. Briefly, RNs were homogenized in Buffer A (320mM sucrose, 1mM EDTA, 50mM TRIS-HCl, pH = 7.4, 1mM DTT, and 1mM PMSF), with protease inhibitor cocktail (Sigma, P8340) by 30 strokes with a glass Pyrex micro homogenizer (Sigma). The homogenate was centrifuged at 1000 × g for 10 min, and the resulting supernatant was centrifuged at 10,000 × g for 20 min to obtain the mitochondrial pellet and the supernatant. The mitochondria-containing pellet was washed three times with buffer B (250mM sucrose, 1mM EGTA–Sigma, E3889, 10mM TRIS-HCl pH = 4) by centrifugation for 10 min at 10,000 × g. The supernatant was centrifuged at 100,000 × g for 1h to generate the cytosolic fraction. Proteins were applied to SDS-PAGE and electroblotted on a PVDF or nitrocellulose membrane. Immunoblotting analysis was performed using chemiluminescence detection kit. The relative levels of immunoreactivity were determined by densitometry using ImageJ software (NIH; USA). Samples were incubated overnight with the following primary antibodies: rabbit anti-JNK (1:500, #sc-571, Santa Cruz), mouse anti-p-JNK (1:500, #sc-6254, Santa Cruz), mouse Anti-Vinculin (1:1000, V9131, Merck), mouse anti-Cytochrome-c (1:1000, BD Pharmingen, UK), mouse anti-ß-Actin (1:1000, #A2228, Sigma), mouse anti-GAPDH (1:1000, Abcam, #ab8245), rabbit anti-Plexin A1 (1:1000, #AB23391, Abcam), rabbit anti-Plexin A2 (1:1000, #AB39357, Abcam), goat anti-mSemaphorin6C (1:250, #AF2108, R&D). Membranes were then incubated with the appropriate horseradish peroxidase-conjugated secondary antibodies (1:3000, Biorad). Immunoreactive bands were detected by using an enhanced chemiluminescence kit (ECL; Amersham Biosciences).

Immunofluorescence and confocal analysis

Mice were perfused as above. For immunofluorescence brains were cut into four series of 30µm-thick coronal sections by means of a freezing microtome and were collected in PB for immunofluorescence experiments. Sections were incubated with a cocktail of primary antibodies, including mouse anti-NeuN (1:200, #MAB377, Merck), rabbit anti-GFAP (1:600, #AB9598, Merck), goat anti-Iba1 (1:600, #NB100-1028, Novus), rabbit anti-Olig2 (1:200, #ab109186, Abcam), rabbit anti-Cleaved Caspase3 (1:200, #9664S, CST); rat anti-CD68 (1:500, #MCA1957T, Biorad); rabbit anti-Plexin A2 (1:300, #AB39357, Abcam). All primary antibody solutions were prepared in PB and 0.3% Triton X-100 and were incubated 48h at 4°C. Each incubation step was followed by three, 5-min rinses in PB. Afterwards, sections were incubated 2h at RT with a cocktail of secondary antibodies, including Alexa Fluor 488 conjugated donkey anti-mouse, Alexa Fluor 488 conjugated donkey anti-rat, Alexa Fluor 488 conjugated donkey anti-rabbit, Alexa Fluor 543 conjugated donkey anti-rabbit, and Alexa Fluor 488 conjugated donkey anti-goat (1:200, Thermo Fisher). Sections were 4,6-diamidino-2-phenylindole (DAPI) counterstained (1:1000; Sigma). In general, sections processed for double/triple immunofluorescence were examined under a confocal laser scanning microscope (Nikon, Eclipse, Ti2, Germany) equipped with four laser lines: violet diode emitting at 405 nm (for DAPI), argon emitting at 488 nm, and helium/neon emitting at 543 nm and 633. To assess microglial and astrocytic count within PN, quantitative analyses were performed off-line on confocal images acquired through the 20× objective at the 1 zoom factor. Three digital square frames (200×200µm) were placed at a regular distance to sample the entire medio-lateral extent of PN. Only immunolabeled cells with a distinct nucleus (DAPI+) in the focal plane were counted[43]. The optical

density (O.D.) was performed by densitometric analyses manually outlining individual cells and measuring cell-associated fluorescence intensity with the ImageJ software (http://rsb.info.nih.gov/ij/). The Mean/Area ratio defines mean fluorescence of individual cells normalized to total cellular surface. Quantification was done on 50 cells per mice. All quantitative analyses were conducted blind to the animal's experimental group assignment.

Sholl analysis

Microglia in the PN were imaged using a fluorescence microscope (Zeiss) equipped with a motorized stage and a camera connected to software (Neurolucida 7.5, MicroBright-Field) that allowed a quantitative 3D analysis of the entire compartment. Only microglia that displayed intact processes unobscured by background labeling or other cells were included in reconstructions. Fifteen cells per animal were randomly selected and included for analysis. The cell body area and perimeter, number of intersections (the number of microglia branches that intersect/cross the radius), number of nodes and total length of all processes were measured[42]. All experiments and data analyses were conducted by experimenters' blind to the groupings.

Cell culture, hydrogen peroxide treatment and Incucyte assay

Neuro-2a (N2a) cells are routinely cultured in Dulbecco's Modified Eagle Medium (DMEM) supplemented with 10% Fetal Bovine Serum (FBS, EuroClone), 2 mM L-glutamine (Sigma-Aldrich) and 1% Penicillin-Streptomycin (EuroClone). Cells were periodically checked for mycoplasma contamination and grown in a 37°C humidified atmosphere of 5% CO2. 12h post seeding cells were transiently silenced with lipofectamine 3000 (Thermo Fischer, #L3000015) with scramble control siRNA (Sigma, SIC002-10nmol), siRNA for Sema6c (Sigma, SASI_MM02_0032–0497) and siRNA for Plxna2 (Sigma, SASI_MM01_0005-3042). After 6hs, medium was changed, and 100uM hydrogen peroxide (H2O2) treatment was added together with Incucyte® Caspase-3/7 green Dye for Apoptosis (Sartorius, #4440). The assay was performed with the IncuCyte SX5 Live-content imaging system (Essen Bioscience) by measuring both phase and green fluorescence every 3hs. Nine fields per well were acquired and the number of cells counted. The ratio between the number of green cells over the number of total cells in percentage respect to siScr was plotted.

Cell culture, overexpression and Co-Immunoprecipitation

HEK-293T and COS-7 cell lines were cultured in DMEM (Sigma-Aldrich) supplemented as stated above. The cells were periodically checked for mycoplasma contamination and grown in a 37°C humidified atmosphere of 5% CO2. Briefly, overexpression of Semaphorin6C and PlexinA2 constructs (produced by gene synthesis by BioCat GmbH, Heidelberg, Germany) were transiently transfected in COS-7 cells by DEAE-Dextran method, while HEK-293T cells were transfected using the calcium chloride (CaCl2) method. 24hs after transfection cells were scraped in IP buffer (Tris HCl pH 7.5 50mM, NaCl 150mM, EDTA 1mM and NP-40 1%) supplemented with protease inhibitor cocktail (Sigma, #P8340), lysates were incubated on a rotator for 20min at + 4°C, were centrifugated at 13000rpm for 10min at + 4°C and

supernatants were collected. 500ug were immunoprecipitated, after 1h of preclearing, for 2h at 4°C. Dynabeads protein G (Thermo Fisher, #10004D) were added for 1hr at 4°C. Beads were recovered, washed 4 times for 5min, resuspended in lysis buffer and heated 5min at 95°C ready for denaturation prior to western blot analysis.

Experimental design and statistical analysis

The number of animals used in each experiment is listed in the figure legend section. The numbers of animals used for biochemical analysis (Wb and qRT-PCR), NSS, and morphological analysis were based on our previous experience with the techniques and on the basis of a sample size calculation performing a power analysis (G Power 3.1 software). In all cases, we assumed a probability equal to 0.05 and a test power equal to 95%, while Δ and standard deviations were based on previous experiments from our group. For statistical analyses, t-test or one-way, two-way (multiple groups) or repeated-measure analysis of variance (ANOVA) followed, in cases of significance, by a Bonferroni post hoc test was applied. See figure legends for more details. Values of $p \leq 0.05$ were considered to be statistically significant. In the box-and-whisker plots, the center line denotes the median value, edges are upper and lower quartiles, whiskers show minimum and maximum values and points are individual experiments. Statistical analyses were carried out by GraphPad Prism 9.0 (GraphPad software for Science, San Diego, CA). All quantitative analyses were conducted blind to the animal's experimental groups.

Results

Cell-type–specific upregulation of Sema6C in the Pontine Nucleus following HCb lesion

To investigate the molecular mechanisms underlying remote response to axonal damage, we used a well-established HCb mouse model (Fig. 1A), in which surgical removal of right cerebellar hemisphere induces degeneration of axotomized neurons located in the pontine nucleus (PN)[10, 11].

Label-free proteomic analysis was performed on PN samples collected at 7 days after HCb and compared with unlesioned control mice (CTRL) revealed broad lesion-induced changes, with 286 significantly upregulated (Abundance Ratio > 1.5, $p < 0.05$) and 269 significantly downregulated proteins (Abundance ratio < 0.66, $p < 0.05$) in HCb mice compared with CTRL (Fig. 1B). Pathway enrichment analysis of the differentially modulated proteins confirmed alterations in metabolism and mitochondrial function, consistent with our previous studies[8, 11]. Interestingly, our analysis further revealed the modulation of pathways related to L1 cell adhesion molecule (L1CAM) ("L1CAM interactions" and "Recycling pathway of L1") and Rho GTPases ("Rho GTPases activate IQGAPs" and "Rho GTPases activate PKNs") (Fig. 1C). Notably, the genes contributing to these pathways mainly encode cell-adhesion molecules, cytoskeletal components, and regulators of membrane trafficking, all processes that are closely linked to axon guidance and structural remodeling. In light of these findings and building

on our long-standing work on semaphorin-mediated mechanisms, we next investigated whether semaphorin signaling may be re-engaged in the PN following HCb-induced axonal damage.

To this aim, we performed bulk mRNA expression analysis in the PN of CTRL and HCb-lesioned mice for a selected panel of Semaphorins. This panel included semaphorins previously implicated in CNS axonal injury such as Sema3A[44, 45], Sema4D[46, 47], Sema7A[48] as well as class 6 Semaphorins, which remain comparatively less characterized in the context of CNS injury but represent plausible candidates for regulating post-lesional responses[49, 50]. Among the Semaphorin transcripts examined, Sema3a, Sema4d, Sema6a, Sema6b, and Sema6d and Sema7a, were not significantly altered following HCb (Suppl. Figure 1A). In contrast, Sema6c mRNA showed a modest increase in HCb mice compared to CTRL animals, with a consistent trend that however did not reach statistical significance ($p = 0.0567$; Fig. 1D). Because bulk analysis may obscure cell-type-specific changes within the heterogeneous post-lesional PN, we next performed RNAscope in situ hybridization to localize Sema6c transcripts with cellular resolution. This analysis revealed a significant upregulation of Sema6c mRNA in the PN of HCb mice compared with CTRL (Fig. 1E, f; $p < 0.0001$). Time-course analysis further showed a progressive increase in Sema6c expression after lesion, peaking at 7 days and remaining elevated up to 21 days (Fig. 1G). Confocal analysis further indicated that the lesion-induced increase in Sema6c expression was mainly associated with neuronal cells (Fig. 1H). In contrast, astrocytes (Suppl. Figure 1B) and microglia (Suppl. Figure 1C) as well as oligodendrocytes (Suppl. Figure 1D) not only did not express Sema6c at basal level but also showed a limited increase in Sema6c mRNA signal, suggesting that non-neuronal cells contribute only marginally to the overall Sema6c upregulation observed after HCb.

Sema6C upregulation promotes JNK-mediated apoptotic cell death following HCb lesion

The HCb model represents a well-established paradigm of remote neurodegeneration, in which injury to synaptically connected, but anatomically distant, brain regions trigger progressive neuronal loss through apoptotic mechanisms[11, 39]. To define the role of Sema6C in this process, we examined the temporal relationship between Sema6c expression and apoptosis after HCb.

Stereological analysis of Nissl-stained neurons revealed a modest reduction as early as 1- and 2-days post-lesion compared with CTRL (Fig. 2A; $p < 0.05$), followed by a progressive decline to approximately 70% of CTRL levels by day 4 and 40% by day 21 (Fig. 2A). This temporal profile appeared complementary to the RNAscope pattern of Sema6c expression (Fig. 1F), suggesting a possible link between Sema6C upregulation and remote neuronal death.

Because HCb-induced degeneration proceeds through a phosphorylated JNK (p-JNK) mediated apoptotic mechanism[11], we next sought to define whether Sema6C is involved in this event. Subsequent analyses were therefore focused on day 4 post-lesion, a time point at which neuronal death was already detectable but still in an early phase, with approximatively 30% of neurons lost.

At this time point, we observed a pronounced increase in phosphorylated JNK (p-JNK) levels within the PN of HCb mice compared with CTRL (Fig. 2B; $p < 0.001$), accompanied by enhanced cytochrome-c release in the cytosol (Fig. 2C; $p < 0.001$). In addition, confocal analysis of immunofluorescent samples revealed a significant increase of cleaved caspase-3 level in the axotomized neurons respect to CTRL (Fig. 2D, E; $p < 0.0001$), confirming the activation of the JNK-mediated apoptotic pathway[11].

To investigate the functional contribution of Sema6C to remote injury-induced neurodegeneration we performed *in vivo* knockdown of Sema6c (HCb 4d-siSema6c group). Efficient knockdown was confirmed by RNAscope (Suppl. Figure 2A, B). Since HCb 4d-siScr mice showed responses comparable to HCb mice across experiments, subsequent analyses are presented relative to the HCb group.

While Sema6c silencing had no effects in unlesioned animals (Suppl. Figure 2C, D), it significantly increased neuronal survival (Fig. 2G, $p < 0.001$) and improved functional recovery compared to HCb (Fig. 2H; Day1: $p < 0.01$; Day4: $p < 0.0001$). In contrast, scramble siRNA (siScr) into HCb-lesioned mice did not affect neuronal survival or NSS compared with CTRL mice, confirming that the observed effects were attributable to specific Sema6C silencing rather than siRNA administration *per se* (Suppl. Figure 2E, F). Notably, Sema6c knockdown reduced JNK phosphorylation (Fig. 2I, $p < 0.05$) and cleaved caspase-3 levels (Fig. 2J, K, $p < 0.0001$). Together, these findings indicate that injury-induced Sema6C upregulation contributes to remote neuronal death, either directly or indirectly, through a JNK-dependent apoptotic pathway.

Exacerbation of remote injury–induced neurodegeneration by recombinant Sema6C injection

To assess the functional impact of aberrant Sema6C signaling and whether its increased extracellular levels may influence neuronal responses to injury, the recombinant extracellular domain of Sema6C (rSEMA6C) was administered via intracerebroventricular (i.c.v.) injection immediately before HCb (Fig. 3A).

In CTRL animals, rSEMA6C did not significantly affect neuronal survival or NSS, indicating that elevated Sema6C levels are not detrimental under physiological conditions (Suppl. Figure 3A, B). In HCb mice, vehicle injection (HCb 4d + PBS) did not affect neuronal survival or NSS compared with untreated HCb animals (Suppl. Figure 3C, D). Therefore, since HCb 4d + PBS group consistently showed responses comparable to untreated HCb mice, rSEMA6C effects are presented relative to the HCb group.

In HCb mice, rSEMA6C significantly worsened NSS (Fig. 3B $p < 0.0001$) and reduced neuronal survival (Fig. 3C $p < 0.01$).

To investigate the global molecular changes induced by recombinant Sema6C administration, we performed proteomic analysis. In the HCb 4d +rSEMA6C group compared with HCb 4d mice, we identified 281 upregulated proteins (Abundance Ratio > 1.5, $p < 0.05$) and 229 downregulated proteins (Abundance ratio < 0.66, $p < 0.05$) (Fig. 3D). Pathway enrichment analysis revealed a significant

downregulation of mitochondrial-related pathways (Fig. 3E). Together with the decreased neuronal survival observed in rSEMA6C-treated mice (see Fig. 3C), these findings suggest that rSEMA6C exacerbates lesion-induced mitochondrial dysfunction and may promote the activation of pro-apoptotic mechanisms. Consistently, cleaved caspase-3 immunostaining was significantly increased in rSEMA6C-lesioned mice, both in terms of positive staining (Fig. 3F) and optical density (Fig. 3G; $p < 0.05$), supporting the overactivation of apoptotic pathways.

Given the association between apoptosis, neuronal loss and altered neuroinflammation[43], we next assessed glial responses by immunofluorescence. Immunofluorescence analysis showed enhanced glial reactivity in rSEMA6C-lesioned mice than in HCb mice (Fig. 3H), with significantly higher numbers of Iba1-positive microglia and GFAP-positive astrocytes than in HCb mice (Fig. 3I, J; $p < 0.0001$). Moreover, within the PN of rSEMA6C-injected lesioned mice, Iba1-positive microglia displayed a more complex morphology than those observed in HCb mice, including enlarged soma size (Fig. 3K, L, $p < 0.0001$) and longer processes, particularly in regions proximal to the cell body (Suppl. Figure 3E). Consistent with the acquisition of a phagocytic phenotype, CD68/Iba1 immunofluorescence showed a significant increase in CD68-positive microglia in rSEMA6C- lesioned mice compared with HCb mice (Fig. 3M-N, $p < 0.0001$), further suggesting an enhanced phagocytic/lysosomal activation state and an exacerbated neuroinflammatory response following rSEMA6C administration.

PlexinA2 Mediates Sema6C Signaling in Pontine Neurons Following HCb lesion

Sema6C is a transmembrane semaphorin that signals through Plexin A receptors, although its specific cognate receptor remains debated. Because Plexin A1 and Plexin A2 are the most plausible candidates, we examined their potential involvement in Sema6C-dependent remote neurodegeneration. qPCR and western blot analyses showed that, after HCb, only Plexin A2 was significantly increased both at mRNA (Fig. 4A, $p < 0.05$) and protein levels (Fig. 4C, $p < 0.05$), whereas Plexin A1 remained unchanged at both the transcript (Fig. 4B) and protein levels (Fig. 4D).

Immunofluorescence showed that Plexin A2 signal was selectively localized within the neuronal compartment (Fig. 4E), with significantly increased immunoreactivity in HCb mice compared with CTRL animals (Fig. 4F, $p < 0.0001$).

To assess whether Sema6C can directly interact with Plexin A2 and to validate receptor specificity, we employed an *in vitro* system and performed co-immunoprecipitation (co-IP) assays following transient overexpression of Sema6C and Plexin A2 in HEK293T cells. These experiments revealed a specific interaction between Sema6C and Plexin A2 (Fig. 4G, H), whereas no interaction was detected with Plexin A1 (Suppl. Figure 4A), strongly suggesting Plexin A2 as the primary receptor mediating Sema6C-dependent signaling in our experimental model. To determine whether activation of this signaling axis has direct consequences on neuronal viability and apoptotic cell death *in vitro*, we next performed live-cell imaging experiments using the IncuCyte platform on Neuro-2A (N2A) cell line. Cells were silenced for Sema6c, for Plxna2, and for both, later exposed to hydrogen peroxide, and then monitored for 24h

with IncuCyte® Apoptosis Assay. Cell viability and apoptotic green fluorescence were then quantified. Consistently, siSema6c treatment, but also siPlxna2 and the combination of the two, significantly decreased the percentage of cleaved caspase-3 + cells when comparing to scrambled siRNA-treated controls, indicating that interference with this axis attenuates activation of the apoptotic cascade (Fig. 4I and Suppl. Figure 4B; siScr vs siSema6c, $p < 0.001$; siScr vs siPlxna2, $p < 0.05$; siScr vs siSema6c-Plxna2, $p < 0.01$).

Next, to determine whether Plexin A2 is required for Sema6C-dependent signaling *in vivo*, we assessed the effect of Plxna2 knockdown after HCb. siRNA targeting Plxna2 was stereotaxically delivered into the PN before lesion, and mice were analyzed at 4 days post-HCb, when early neuronal loss, Sema6C upregulation, and apoptotic signaling are evident. Efficient reduction of Plexin A2 protein was confirmed by immunofluorescence in siPlxna2 lesioned mice compared with scrambled siRNA HCb-mice (Fig. 4J, K, $p < 0,0001$). In unlesioned animals, Plxna2 knockdown did not significantly affect neuronal survival and neurological functions (NSS) (Suppl. Figure 4C, D), suggesting that Plexin A2, like Sema6C, is dispensable for baseline neuronal maintenance.

As observed for Sema6c silencing, the HCb 4d + siScr mice showed responses comparable to untreated HCb animals across all experimental readouts (data not shown). Therefore, Plxna2 knockdown analyses are presented relative to the HCb group.

Importantly, Plxna2 knockdown in lesioned animals significantly increased neuronal survival (Fig. 4L, $p < 0.001$), reduced cleaved caspase-3 immunoreactivity (Fig. 4M-N, $p < 0,001$), and improved functional recovery (Fig. 4O; 4 Days: $p < 0.0001$), thereby recapitulating the protective effects observed after *in vivo* Sema6c silencing.

Discussion

A major implication of our work is that axonal injury can trigger molecular programs that extend the impact of a focal lesion beyond the primary site of damage. Secondary neurodegeneration is increasingly recognized after stroke, traumatic injury, and other CNS disorders, where it may contribute to progressive tissue loss and long-term disability[3, 51, 52]. This concept is particularly relevant because axonopathy is increasingly viewed not only as a consequence of neuronal death but also as an early and active contributor to disease progression across neurodegenerative conditions, including Alzheimer's disease, Parkinson's disease, Huntington's disease, and amyotrophic lateral sclerosis[53, 54]. In this framework, Sema6C-dependent signaling may represent a mechanism through which injured axons communicate damage to vulnerable neuronal populations and amplify degeneration within connected circuits.

Sema6C belongs to the class 6 semaphorin family, a group of transmembrane guidance molecules involved in nervous system development, axonal pathfinding, and circuit assembly[55, 56]. Structurally, Sema6C is a transmembrane protein considered a distal class 6 semaphorin because of its longer and

partly divergent cytoplasmic domain. This organization is relevant because transmembrane semaphorins can mediate both forward signaling, as ligands for plexin-containing receptor complexes, and reverse signaling through their intracellular domains.

Previous studies have shown that Sema6C is expressed in the developing nervous system, where it exerts growth cone-collapsing and axon-repulsive activity, including in dorsal root ganglion neurons. Its expression in embryonic target tissues, such as the myotome and dermatome, supports a roles in axon navigation, target recognition, axonal arrest, and synapse formation. In adult tissues, Sema6C is enriched in the brain and skeletal muscle[57], where it may contribute to neuromuscular junction stability[58]. Our findings extend this framework by showing that Sema6C is re-engaged in the adult injured CNS, where its activity is associated with neuronal degeneration rather than adaptive remodeling.

The finding that Sema6C promotes neuronal death after axonal injury supports the broader concept that developmental guidance cues can acquire pathological functions in the adult nervous system[59]. Molecules originally involved in axon navigation and circuit formation are increasingly recognized as regulators of CNS plasticity, neuroinflammation, and injury responses[60, 61]. This duality is well illustrated by semaphorin signaling, whose effects depend on receptor composition, cellular context, developmental stage, and disease state[27, 60]. Accordingly, several semaphorins, including Sema3A, Sema3E, and Sema4B, regulate not only neuronal growth and guidance but also neuroimmune and neurodegenerative mechanisms[19, 30, 31, 62]. Thus, the deleterious effect of Sema6C in axotomized neurons is consistent with the functional plasticity of the semaphorin family and suggests that Sema6C participates in injury-specific signaling programs distinct from its developmental roles.

Transmembrane semaphorins can signal through multiple mechanisms[63]. They may interact with receptors or surface molecules on neighboring cells, act at a distance after proteolytic shedding, or signal through their own intracellular domains via reverse signaling. In the case of Sema6C, these mechanisms have remained largely unexplored. Our data address this gap, by showing that the detrimental effects of Sema6C after axonal injury are mediated, at least in part, through PlexinA2. Notably, the data shown in this work indicate that the pro-apoptotic activity of Sema6C in PlexinA2-overexpressing injured neurons is mediated by forward signaling, since it can be recapitulated by the soluble extracellular domain of the semaphorin.

Plexin A2 is an A-type plexin receptor that couples extracellular guidance cues to intracellular pathways regulating cytoskeletal dynamics, cell adhesion, neuronal morphology, and cell fate[64, 65]. Plexin A2 has also been linked to mechanisms limiting axonal sprouting and functional recovery after CNS trauma, including Nogo-A/NgR1/CRMP2 signaling complexes[66]. Our findings extend this role by identifying Plexin A2 as a receptor mediating Sema6C-dependent neurodegeneration in axotomized neurons. Mechanistically, we show that Sema6C/Plexin A2 signaling converges on JNK phosphorylation and activation. JNK is a central stress-activated kinase pathway in the CNS, implicated in axonal injury responses, cytoskeletal remodeling, mitochondrial dysfunction, inflammatory signaling, and apoptosis[67].

Sustained JNK activation can promote neuronal death through c-Jun activation, regulation of Bcl-2 family members, and mitochondrial apoptotic signaling[11, 68, 69]. In our model, Sema6C upregulation and increased phosphorylated JNK support a mechanistic link between Sema6C/Plexin A2 activation and injury-induced neuronal death.

JNK involvement may also explain the broader pathological phenotype observed after Sema6C activation. Beyond cell-autonomous apoptosis, JNK signaling can shape inflammatory responses, glial activation, and injury-induced remodeling[70, 71]. Accordingly, the exacerbation of inflammatory responses after recombinant Sema6C administration suggests that Sema6C/Plexin A2/JNK signaling may contribute to a feed-forward degenerative loop. In this model, axonal injury induces Sema6C in vulnerable neurons; soluble or membrane-associated Sema6C engages Plexin A2; JNK activation promotes neuronal apoptosis and stress signaling; and neuronal damage further enhances local neuroinflammation. Such a mechanism could amplify the consequences of focal CNS injury and contribute to delayed functional deterioration.

The biological activity of recombinant Sema6C also raises the possibility that a soluble extracellular form, potentially generated by ectodomain shedding, contributes to injury-signal propagation[63]. However, because Sema6C shedding has not yet been directly demonstrated, future studies should determine whether soluble Sema6C is generated after injury and whether it contributes to neuroinflammatory amplification and secondary neurodegeneration.

The reciprocal effects obtained through genetic and pharmacological modulation strengthen the causal interpretation of our findings. Sema6C silencing reduced neuronal death and improved behavioral recovery, whereas recombinant Sema6C worsened neuropathological and functional outcomes. These results suggest that Sema6C is not merely a marker of axotomized neurons but an actionable component of the degenerative cascade.

From a translational perspective, the Sema6C/Plexin A2/JNK axis may offer several opportunities. Sema6C could serve as a marker of neurons undergoing maladaptive responses to axonal injury, while Plexin A2-dependent signaling may provide a targetable receptor-level mechanism linking injury-induced semaphorin signals to intracellular stress responses. Pathway engagement could be monitored through downstream readouts such as phosphorylated JNK, neuroinflammatory markers, and axonal injury biomarkers. Therapeutic strategies aimed at interrupting this pathway may act upstream of neuronal apoptosis and inflammatory amplification, potentially expanding the therapeutic window for limiting secondary degeneration in disorders characterized by axonal damage. Notably, the clinical testing of a humanized antibody blocking Sema4D signaling in neurodegenerative disease[32] supports the feasibility of therapeutically targeting semaphorin pathways, including Sema6C. However, several questions remain. Future studies should determine whether Sema6C is induced in other CNS injury models and in chronic neurodegenerative conditions with prominent axonopathy, define the injury-related signals and transcriptional programs controlling its expression, and validate the clinical relevance of this pathway in human tissue, biofluid biomarkers, or patient-derived cellular systems.

In conclusion, our study identifies Sema6C/PlexinA2 signaling as a novel injury-induced pathway linking axonal injury to secondary neurodegeneration through JNK activation, neuronal apoptosis, neuroinflammatory amplification. Thus, the Sema6C/Plexin A2/JNK axis emerges as a promising target to limit secondary degeneration and improve functional recovery after CNS injury.

Abbreviations

Cyt-c
cytochrome-c
CNS
central nervous system
DAPI
4,6-diamidino-2-phenylindole
GFAP
glial fibrillary acidic protein
HCb
hemicerebellectomy
i.c.v.
intracerebroventricular
NSS
Neurological Severity Score
O.D.
optical density
PB
phosphate-buffer
Plxn
Plexin
PN
pontine nuclei
Semas
semaphorins
Scr
scramble

Declarations

Acknowledgements

We thank Claudia Palazzo, Roberta Mastrantonio, Sara Delmirani, Emanuele Valzano and Elena Musumeci for their valuable help and support.

Funding

This work was supported by Linea D.1. 2024-25 (R4124501168) Università Cattolica del S. Cuore (to M.T.V.).

Contributions

S.N., D.P. and M.T.V. conceived and designed the research. S.N., F.R., V.G. and A.P. performed the experiments and carried out the statistical analyses. S.N., F.R., D.P. and M.T.V. analyzed and interpreted the data. D.P., L.T., A.U. and M.T.V. supervised the study and contributed to manuscript review and editing. S.N., D.P. and M.T.V. drafted and wrote the manuscript. All authors critically revised the manuscript for important intellectual content, read and approved the final version.

Ethics declarations

Ethics approval and consent to participate. All animal studies complied with all relevant ethical regulations for animal testing and research and were approved by the Italian Ministry of Health (Prot. Number:436/2024-PR).

Competing interests

The authors declare that they have no competing interests.

Data availability

Data generated or analysed during this study are included in this published article and its supplementary information files. The mass spectrometry proteomics data will be deposited in the ProteomeXchange Consortium via the PRIDE partner repository upon acceptance of the manuscript.

During the peer-review process, the data are available upon request.

Supplementary information

Supplementary information accompanies the manuscript.

References

1. Richards LJ, Huang C, Bauer AQ, Lee JM. Long-range axon branching: contributions to brain network plasticity and repair. *Nat Rev Neurosci.* 27, 243–259 (2026).
2. Viscomi MT, Oddi S, Latini L, Bisicchia E, Maccarrone M, Molinari M. The endocannabinoid system: A new entry in remote cell death mechanisms. *Exp Neurology* 224, 56–65 (2010).
3. Viscomi MT, Molinari M. Remote Neurodegeneration: Multiple Actors for One Play. *Mol Neurobiol* 50, 368–389 (2014).

4. Lingor P, Koch JC, Tönges L, Bähr M. Axonal degeneration as a therapeutic target in the CNS. *Cell Tissue Res* 349, 289–311 (2012).
5. Medana IM, Esiri MM. Axonal damage: a key predictor of outcome in human CNS diseases. *Brain* 126, 515–530 (2003).
6. Rishal I, Fainzilber M. Axon–soma communication in neuronal injury. *Nat Rev Neurosci* 15, 32–42 (2014).
7. Abe N, Cavalli V. Nerve injury signaling. *Curr Opin Neurobiol* 8, 276–283 (2008).
8. Cavallucci V, Bisicchia E, Cencioni MT, Ferri A, Latini L, Nobili A, et al. Acute focal brain damage alters mitochondrial dynamics and autophagy in axotomized neurons. *Cell Death Dis* 5, e1545-e1545 (2014).
9. Oddi S, Latini L, Viscomi MT, Bisicchia E, Molinari M, Maccarrone M. Distinct regulation of nNOS and iNOS by CB2 receptor in remote delayed neurodegeneration. *J Mol Med* 90, 371–387 (2012).
10. Viscomi MT, D'Amelio M, Cavallucci V, Latini L, Bisicchia E, Nazio F, et al. Stimulation of autophagy by rapamycin protects neurons from remote degeneration after acute focal brain damage. *Autophagy* 8, 222–235 (2012).
11. Viscomi MT, Oddi S, Latini L, Pasquariello N, Florenzano F, Bernardi G, et al. Selective CB2 Receptor Agonism Protects Central Neurons from Remote Axotomy-Induced Apoptosis through the PI3K/Akt Pathway. *J Neurosci* 8, 4564–4570 (2009).
12. Hollis ER, Ishiko N, Yu T, Lu CC, Haimovich A, Tolentino K, et al. Ryk controls remapping of motor cortex during functional recovery after spinal cord injury. *Nat Neurosci* 19, 697–705 (2016).
13. Li L, Hutchins BI, Kalil K. Wnt5a Induces Simultaneous Cortical Axon Outgrowth and Repulsive Axon Guidance through Distinct Signaling Mechanisms. *J Neurosci* 29, 5873–5883 (2009).
14. Liu Y, Wang X, Lu CC, Sherman-Kermen R, Steward O, Xu XM, et al. Repulsive Wnt Signaling Inhibits Axon Regeneration after CNS Injury. *J Neurosci* 28, 8376–8382 (2008).
15. Liu Y, Shi J, Lu CC, Wang ZB, Lyuksyutova AI, Song XJ, et al. Ryk-mediated Wnt repulsion regulates posterior-directed growth of corticospinal tract. *Nat Neurosci* 8, 1151–1159 (2005).
16. Jeroen Pasterkamp R, Peschon JJ, Spriggs MK, Kolodkin AL. Semaphorin 7A promotes axon outgrowth through integrins and MAPKs. *Nature* 424, 398–405 (2003).
17. Kolodkin AL, Matthes DJ, Goodman CS. The semaphorin genes encode a family of transmembrane and secreted growth cone guidance molecules. *Cell* 75, 1389–1399 (1993).
18. Pasterkamp RJ, Kolodkin AL. Semaphorin junction: making tracks toward neural connectivity. *Curr Opin Neurobiology* 13, 79–89. (2003).
19. Good PF, Alapat D, Hsu A, Chu C, Perl D, Wen X, et al. A role for semaphorin 3A signaling in the degeneration of hippocampal neurons during Alzheimer's disease. *J Neurochem* 91, 716–736 (2004).
20. Moreau-Fauvarque C, Kumanogoh A, Camand E, Jaillard C, Barbin G, Boquet I, et al. The Transmembrane Semaphorin Sema4D/CD100, an Inhibitor of Axonal Growth, Is Expressed on

Oligodendrocytes and Upregulated after CNS Lesion. *J Neurosci* 23, 9229–9239 (2003).

21. Ben-Zvi A, Ben-Gigi L, Yagil Z, Lerman O, Behar O. Semaphorin3A regulates axon growth independently of growth cone repulsion via modulation of TrkA signaling. *Cell Signal* 20, 467–479 (2008).
22. Ben-Zvi A, Manor O, Schachner M, Yaron A, Tessier-Lavigne M, Behar O. The Semaphorin Receptor PlexinA3 Mediates Neuronal Apoptosis during Dorsal Root Ganglia Development. J *Neurosci* 28, 12427–12432 (2008).
23. Giger RJ, Hollis ER, Tuszynski MH. Guidance Molecules in Axon Regeneration. *Cold Spring Harb Perspect Biol* 2, a001867-a001867 (2010).
24. Shirvan A, Kimron M, Holdengreber V, Ziv I, Ben-Shaul Y, Melamed S, et al. Anti-semaphorin 3A Antibodies Rescue Retinal Ganglion Cells from Cell Death following Optic Nerve Axotomy. *J Biol Chem* 277, 49799–49807 (2002).
25. Shirvan A, Ziv I, Fleminger G, Shina R, He Z, Brudo I, et al. Semaphorins as Mediators of Neuronal Apoptosis. *J Neurochem* 73, 961–971 (1999).
26. Nutarelli S, Palazzo C, Viscomi MT. Glia and semaphorins in neurodegenerative diseases: The frontier for new therapeutics. *Neural Reg Res* 21, 2323–2324 (2026).
27. Carulli D, De Winter F, Verhaagen J. Semaphorins in Adult Nervous System Plasticity and Disease. *Front Synaptic Neurosci* 13, 672891 (2021).
28. Palazzo C, Nutarelli S, Mastrantonio R, Tamagnone L, Viscomi MT. Glia–glia crosstalk via semaphorins: Emerging implications in neurodegeneration. *Ageing Res Rev* 104, 102618 (2025).
29. Birger A, Ottolenghi M, Perez L, Reubinoff B, Behar O. ALS-related human cortical and motor neurons survival is differentially affected by Sema3A. *Cell Death Dis* 9, 256 (2018).
30. Casden N, Belzer V, El Khayari A, El Fatimy R, Behar O. Astrocyte-to-microglia communication via Sema4B-Plexin-B2 modulates injury-induced reactivity of microglia. *Proc Natl Acad Sci U S A* 121, e2400648121 (2024).
31. Evans EE, Mishra V, Mallow C, Gersz EM, Balch L, Howell A, et al. Semaphorin 4D is upregulated in neurons of diseased brains and triggers astrocyte reactivity. *J Neuroinflam* 19, 200 (2022).
32. Feigin A, Evans EE, Fisher TL, Leonard JE, Smith ES, Reader A, et al. Pepinemab antibody blockade of SEMA4D in early Huntington's disease: a randomized, placebo-controlled, phase 2 trial. *Nat Med* 28, 2183–2193 (2022).
33. Smith ES, Jonason A, Reilly C, Veeraraghavan J, Fisher T, Doherty M, et al. SEMA4D compromises blood–brain barrier, activates microglia, and inhibits remyelination in neurodegenerative disease. *Neurobiol Dis* 73, 254–268 (2015).
34. Tanelian DL, Barry MA, Johnston SA, Le T, Smith GM. Semaphorin III can repulse and inhibit adult sensory afferents in vivo. *Nat Med* 3, 1398–1401 (1997).
35. Venkova K, Christov A, Kamaluddin Z, Kobalka P, Siddiqui S, Hensley K. Semaphorin 3A Signaling Through Neuropilin-1 Is an Early Trigger for Distal Axonopathy in the SOD1^{G93A} Mouse Model of

Amyotrophic Lateral Sclerosis. *J Neuropathol Exp Neurol* 73, 702–713 (2014).

36. Kikuchi K, Chédotal A, Hanafusa H, Ujimasa Y, De Castro F, Goodman CS, et al. Cloning and Characterization of a Novel Class VI Semaphorin, Semaphorin Y. *Mol Cell Neurosci* 13, 9–23 (1999).
37. Hung YH, Hsu SH, Hou YC, Chu PY, Su YY, Shan YS, et al. Semaphorin 6C Suppresses Proliferation of Pancreatic Cancer Cells via Inhibition of the AKT/GSK3/β-Catenin/Cyclin D1 Pathway. *IJMS* 23, 2608 (2022).
38. Fard D, Testa E, Panzeri V, Rizzolio S, Bianchetti G, Napolitano V, et al. SEMA6C: a novel adhesion-independent FAK and YAP activator, required for cancer cell viability and growth. *Cell Mol Life Sci* 80, 111 (2023).
39. Bisicchia E, Sasso V, Catanzaro G, Leuti A, Besharat ZM, Chiacchiarini M, et al. Resolvin D1 Halts Remote Neuroinflammation and Improves Functional Recovery after Focal Brain Damage Via ALX/FPR2 Receptor-Regulated MicroRNAs. *Mol Neurobiol* 55, 6894–6905. (2018).
40. Distler U, Kuharev J, Navarro P, Tenzer S. Label-free quantification in ion mobility–enhanced data-independent acquisition proteomics. *Nat Protoc* 11, 795–812 (2016).
41. Yu G. Thirteen years of clusterProfiler. *The Innovation* 5, 100722 (2024).
42. Catale C, Bisicchia E, Carola V, Viscomi MT. Early life stress exposure worsens adult remote microglia activation, neuronal death, and functional recovery after focal brain injury. Brain Beh Imm 94, 89–103 (2021).
43. Viscomi MT, Florenzano F, Latini L, Amantea D, Bernardi G, Molinari M. Methylprednisolone treatment delays remote cell death after focal brain lesion. *Neuroscience* 154, 1267–1282 (2008).
44. Pasterkamp RJ, Giger RJ, Ruitenberg MJ, Holtmaat AJGD, De Wit J, De Winter F, et al. Expression of the Gene Encoding the Chemorepellent Semaphorin III Is Induced in the Fibroblast Component of Neural Scar Tissue Formed Following Injuries of Adult But Not Neonatal CNS. *Mol Cell Neurosc*i 13, 143–166 (1999).
45. Kaneko S, Iwanami A, Nakamura M, Kishino A, Kikuchi K, Shibata S, et al. A selective Sema3A inhibitor enhances regenerative responses and functional recovery of the injured spinal cord. *Nat Med* 12, 1380–1389 (2006).
46. Zhou Y, Li Y, Jin H, Wu J, He Q, Wang X, et al. Sema4D/PlexinB1 inhibition ameliorates blood-brain barrier damage and improves outcome after stroke in rats. *FASEB J* 32, 2181–2196 (2018).
47. Zhang HL, Wang J, Tang L. Sema4D knockdown in oligodendrocytes promotes functional recovery after spinal cord injury. *Cell Biochem Biophys* 68, 489–496 (2014).
48. Loy K, Fourneau J, Meng N, Denecke C, Locatelli G, Bareyre FM. Semaphorin 7A restricts serotonergic innervation and ensures recovery after spinal cord injury. *Cell Mol Life Sci* 78, 2911–2927 (2021).
49. Ueno M, Nakamura Y, Nakagawa H, Niehaus JK, Maezawa M, Gu Z, et al. Olig2-Induced Semaphorin Expression Drives Corticospinal Axon Retraction After Spinal Cord Injury. *Cereb Cortex* 30, 5702–5716 (2020).

50. Gu Z, Koppel N, Kalamboglas J, Alexandrou G, Li J, Craig C, et al. Semaphorin-Mediated Corticospinal Axon Elimination Depends on the Activity-Induced Bax/Bak-Caspase Pathway. *J Neurosci* 40, 5402–5412 (2020).
51. Ong LK. Beyond the Primary Infarction: Focus on Mechanisms Related to Secondary Neurodegeneration after Stroke. *IJMS* 23, 16024 (2022).
52. Zhang J, Zhang Y, Xing S, Liang Z, Zeng J. Secondary Neurodegeneration in Remote Regions After Focal Cerebral Infarction: A New Target for Stroke Management? *Stroke* 43, 1700–1705 (2012).
53. Loreto A, Neukomm LJ. Programmed axon degeneration: mechanism, inhibition and therapeutic potential. *Nat Rev Neurosci* 27, 44–60 (2026).
54. Shen R, Sung K, Ding J, Wu C. Axonopathy: mechanisms and potential therapeutic targets for neurodegenerative diseases. *Transl Neurodegener* 15, 13 (2026).
55. Koropouli E, Kolodkin AL. Semaphorins and the dynamic regulation of synapse assembly, refinement, and function. *Curr Opin Neurobiol* 27:1–7 (2014).
56. Limoni G. Modelling and Refining Neuronal Circuits with Guidance Cues: Involvement of Semaphorins. *IJMS* 22, 6111 (2021).
57. Qu X, Wei H, Zhai Y, Que H, Chen Q, Tang F, et al. Identification, Characterization, and Functional Study of the Two Novel Human Members of the Semaphorin Gene Family. *J Biol Chem* 277, 35574–35585 (2002).
58. Svensson A, Libelius R, Tågerud S. Semaphorin 6C expression in innervated and denervated skeletal muscle. *J Mol Hist* 39, 5–13 (2008).
59. Van Battum EY, Brignani S, Pasterkamp RJ. Axon guidance proteins in neurological disorders. *Lancet Neurol* 14, 532–546. (2015).
60. Pasterkamp RJ, Verhaagen J. Semaphorins in axon regeneration: developmental guidance molecules gone wrong? *Phil Trans R Soc B* 361, 1499–1511 (2006).
61. Zheng B, Tuszynski MH. Regulation of axonal regeneration after mammalian spinal cord injury. *Nat Rev Mol Cell Biol* 24, 396–413 (2023).
62. Sweetat S, Casden N, Behar O. Improved neuron protection following cortical injury in the absence of Semaphorin4B. *Front Cell Neurosci* 16, 1076281 (2022).
63. Battistini C, Tamagnone L. Transmembrane semaphorins, forward and reverse signaling: have a look both ways. *Cell Mol Life Sci* 73, 1609–1622 (2016).
64. Negishi M, Oinuma I, Katoh H. Plexins: axon guidance and signal transduction. CMLS, *Cell Mol Life Sci* 62, 1363–1371 (2005).
65. Winberg ML, Noordermeer JN, Tamagnone L, Comoglio PM, Spriggs MK, Tessier-Lavigne M, et al. Plexin A Is a Neuronal Semaphorin Receptor that Controls Axon Guidance. *Cell* 95, 903–916 (1998).
66. Sekine Y, Algarate PT, Cafferty WBJ, Strittmatter SM. Plexina2 and CRMP2 Signaling Complex Is Activated by Nogo-A-Liganded Ngr1 to Restrict Corticospinal Axon Sprouting after Trauma. *J Neurosci* 39, 3204–3216 (2019).

67. De Los Reyes Corrales T, Losada-Pérez M, Casas-Tintó S. JNK Pathway in CNS Pathologies. *IJMS* 22, 3883 (2021).
68. Puthalakath H, O'Reilly LA, Gunn P, Lee L, Kelly PN, Huntington ND, et al. ER Stress Triggers Apoptosis by Activating BH3-Only Protein Bim. *Cell* 129, 1337–1349 (2007).
69. Tabas I, Ron D. Integrating the mechanisms of apoptosis induced by endoplasmic reticulum stress. *Nat Cell Biol* 13, 184–190 (2011).
70. Li X, Cudaback E, Breyer RM, Montine KS, Keene CD, Montine TJ. Eicosanoid receptor subtype-mediated opposing regulation of TLR-stimulated expression of astrocyte glial-derived neurotrophic factor. *FASEB J* 26, 3075–3083 (2012).
71. Zhang S, Cherwinski H, Sedgwick JD, Phillips JH. Molecular Mechanisms of CD200 Inhibition of Mast Cell Activation. *J Immunol* 173, 6786–6793 (2004).

Figures

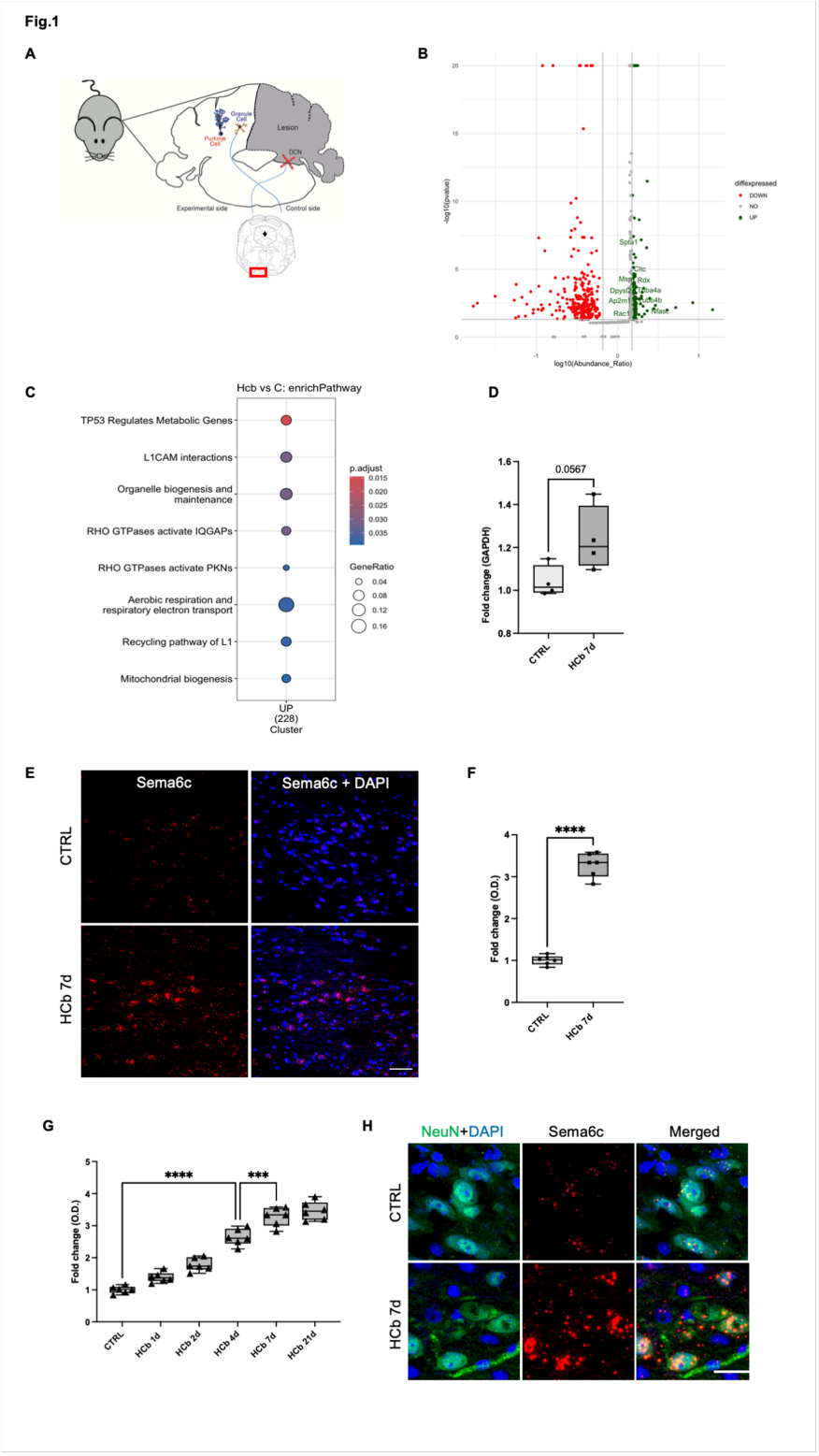

Figure 1

Sema6C is upregulated in the pontine nuclei following hemicerebellectomy. (A) Schematic representation of the hemicerebellectomy (HCb) mouse model. (B) Volcano plot showing differentially modulated proteins in HCb 7d mice compared with controls (CTRL). Upregulated proteins are shown in green, downregulated proteins in red (adjusted $p < 0.05$), and non-significantly modulated proteins in grey. Selected proteins are labelled. (C) Dot plot showing enriched pathways among the differentially

modulated proteins in HCb 7d versus CTRL. (D) Sema6c mRNA expression assessed by qPCR (N = 4/group). (E) Representative RNAscope images showing Sema6c mRNA expression (red) and DAPI counterstaining (blue) in the PN of CTRL and HCb mice 7 days after lesion (HCb 7d). (F) Quantification of Sema6c mRNA signal intensity, expressed as optical density (O.D.) (N = 6/group). Scale bar = 50 μm. (G) Quantification of Sema6c mRNA signal intensity across the indicated time points after HCb, expressed as optical density (O.D.) (N = 6/group). (H) Representative confocal images of RNAscope staining showing Sema6c mRNA expression (red) and NeuN immunostaining (green) in the PN of CTRL and HCb 7d mice. Nuclei were counterstained with DAPI (blue). Scale bar = 25 μm. Box plots indicate median, interquartile range, and min–max values. Each dot represents one animal. *p< 0.05, **p< 0.01, ***p< 0.001, ****p< 0.0001.

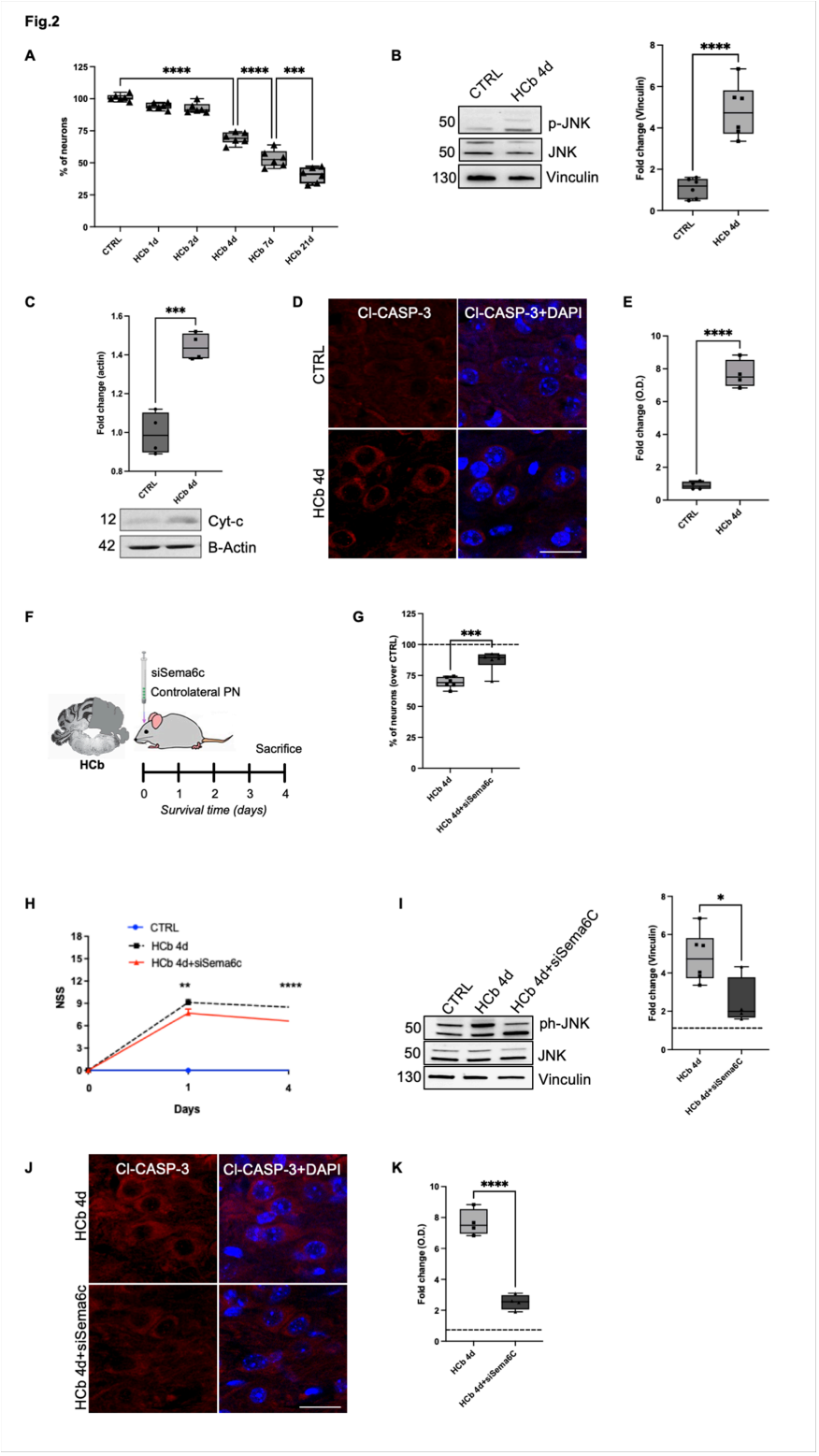

Figure 2

Sema6C contributes to JNK-mediated apoptotic signaling and neuronal loss after hemicerebellectomy. (A) Graph of the quantification of surviving neurons in the PN expressed as the percentage of neurons relative to the CTRL group (N=6/group). (B) Representative Western blot and graph showing total JNK and phosphorylated JNK (p-JNK) protein levels in the different experimental groups (N=6/group). Optical density analysis was performed on both bands. (C) Representative Western blot and graph showing

cytosolic cytochrome-c protein levels in the different experimental groups (N=4/group). (D) Representative confocal images showing cleaved-caspase3 (red) and DAPI (blue) counterstaining in PN of CTRL and HCb 4d. (E) Graph of relative caspase3-signal intensity quantification presented as optical density (O.D.) in the different experimental groups (N=4/group). Scale bar=25μm. (F) Schematic representation of the experimental design. (G) Graph of the quantification of surviving neurons in the PN expressed as percentage of neurons relative to the CTRL (N=6/group). (H) Graph showing the Neurological Severity Score (NSS) of CTRL, HCb 4d and HCb 4d+siSema6c mice. (I) Representative Western blot and graph showing total JNK and phosphorylated JNK (p-JNK) protein levels in the different experimental groups. (N=6 CTRL and HCb 4d). Optical density analysis performed on both bands. (J) Representative confocal images of cleaved-caspase3 (red) and DAPI counterstaining (blue) in PN of HCb 4d+siScr and HCb 4d+siSema6c; (K) Graph of relative caspase3-signal intensity quantification presented as optical density (O.D.) in the different experimental groups respect to the control group (dotted line, fold change=1) (N=4/group). Box plots indicate median, interquartile range, and min–max values. Each dot represents one animal. *p< 0.05, **p< 0.01, ***p< 0.001, ****p< 0.0001.

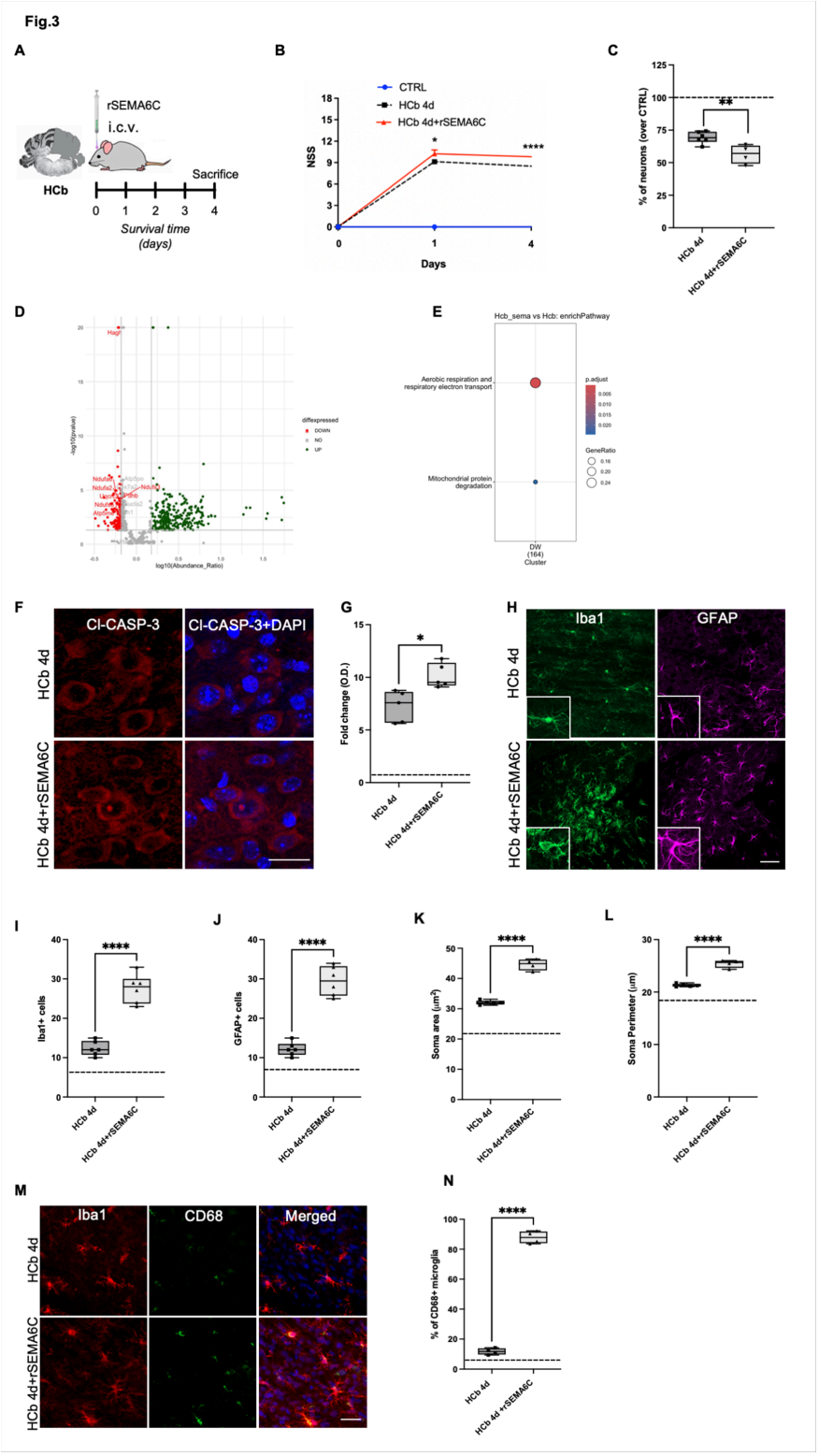

Figure 3

Recombinant SEMA6C worsens neurological deficits, neuronal loss, apoptosis, and glial activation after hemicerebellectomy. (A) Experimental design. (B) Neurological Severity Score (NSS) in CTRL, HCb 4d, and HCb 4d + rSEMA6C mice. (C) Quantification of surviving PN neurons, expressed as percentage of CTRL (N = 4/group). (D) Volcano plot of differentially modulated proteins in HCb 4d + rSEMA6C versus HCb 4d mice; upregulated proteins are shown in green, downregulated proteins in red (adjusted p <

0.05), and non-significant proteins in grey. Selected proteins are indicated. (E) Enriched pathways among differentially modulated proteins. (F) Representative confocal images of cleaved caspase-3 (red) and DAPI (blue) staining in the PN of HCb 4d and HCb 4d + rSEMA6C mice. Scale bar = 25 μm. (G) Quantification of cleaved caspase-3 signal intensity, expressed as optical density (O.D.) relative to CTRL (dotted line; fold change = 1; N = 5/group). (H) Representative confocal images of Iba1 (green) and GFAP immunostaining (magenta) in the PN. Scale bar = 50 μm. (I) Quantification of Iba1+ cells relative to CTRL (dotted line; fold change = 1; N = 5/group). (J) Quantification of and GFAP+ cells relative to CTRL (dotted line; fold change = 1; N = 5/group). (K) Box-and-whisker plots showing microglial soma area after Sholl analysis (N = 4–5/group). Dotted line represents the CTRL. **(**L**)** Box-and-whisker plots showing microglial soma perimeter after Sholl analysis (N = 4–5/group). Dotted line represents the CTRL. (M) Representative confocal images of Iba1 (red) and CD68 (green) staining in the PN. Scale bar = 30 μm. (N) Quantification of CD68+ microglia relative to CTRL (dotted line; fold change = 1; N = 4/group). Box plots show median, interquartile range, and min–max values; each dot represents one animal. *p < 0.05, **p < 0.01, ***p < 0.001, ***p < 0.0001.

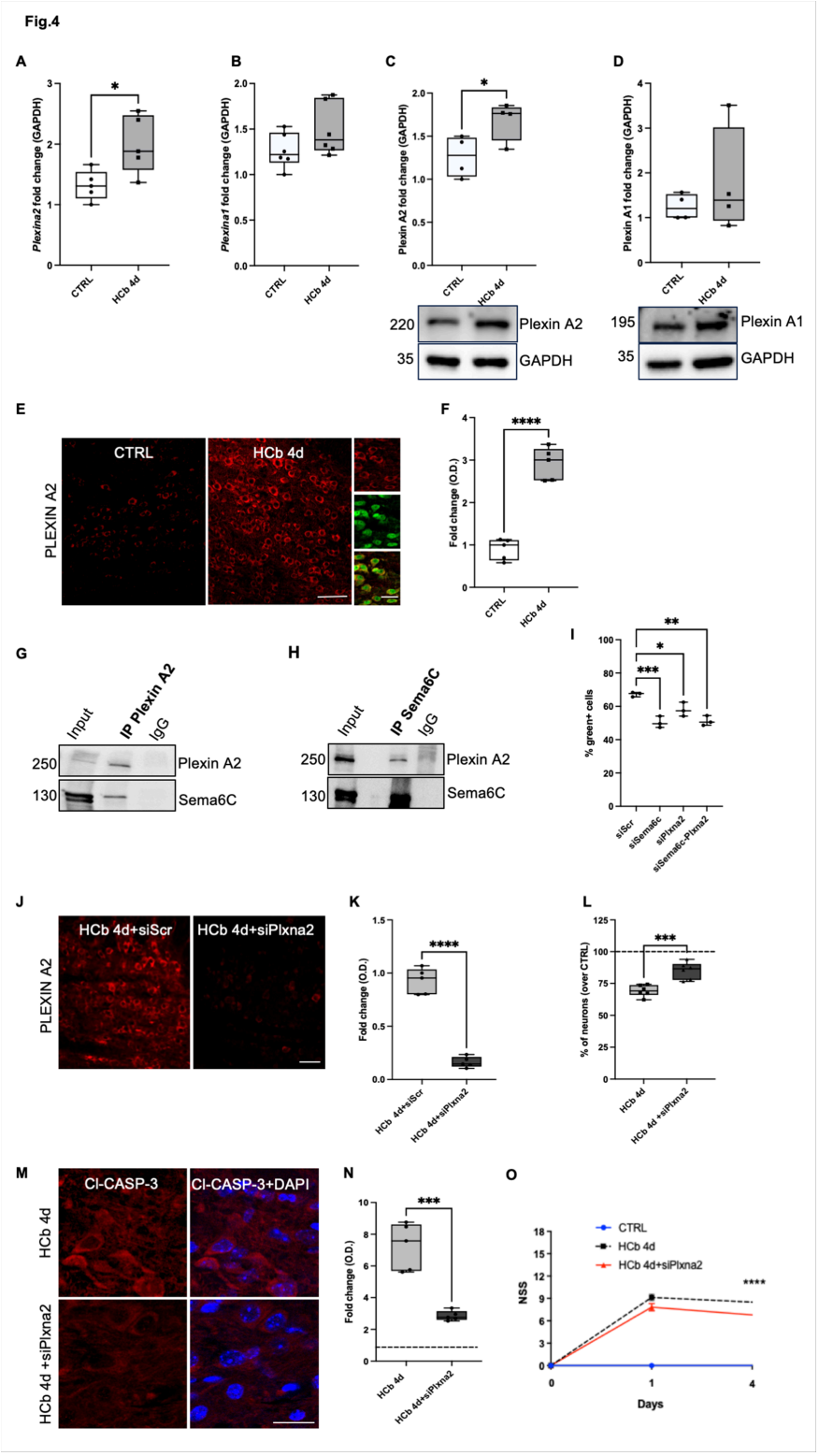

Figure 4

PlexinA2 mediates Sema6C-induced apoptotic signaling, neuronal loss, and neurological impairment after hemicerebellectomy.

(A) Plxna1 mRNA expression assessed by qPCR across experimental groups (N = 4/group). (B) Plxna2 mRNA expression assessed by qPCR across experimental groups (N = 4/group). (C) Representative Western blot of Plexin A1 and quantification across groups (N = 4/group). (D) Representative Western

blot of Plexin A2 and quantification across groups (N = 4/group). (E) Representative confocal images of Plexin A2 (red) and NeuN (green) in PN of CTRL and HCb 4d mice. Scale bar =50 µm and 30 µm (inset). (F) Quantification of Plexin A2 signal intensity expressed as optical density (O.D.) (N = 5/group). (G) Western blot showing interaction between Sema6C and Plexin A2 after Plexin A2 immunoprecipitation in HEK cells overexpressing both proteins. Input corresponds to 10% of extract; IgG used as negative control. Representative of three biological replicates. (H) Western blot showing interaction after Sema6C immunoprecipitation under the same conditions. Input 10%; IgG control; three biological replicates. (I) Percentage of apoptotic cells measured by Incucyte Dye for Apoptosis in H_2O_2-treated N2A cells under siScr, siSema6c, siPlxna2, and combined silencing conditions. Each dot represents one biological replicate. (J) Representative confocal images of Plexin A2 (red) in PN of HCb 4d and HCb 4d + siPlxna2 mice. Scale bar = 50 µm. (K) Quantification of Plexin A2 signal intensity (O.D.) (N = 5/group). (L) Quantification of surviving neurons as percentage of CTRL (N = 4/group). (M) Representative confocal images of cleaved caspase-3 (red) and DAPI (blue) in PN of HCb 4d + siScr and HCb 4d + siPlxna2 mice. Scale bar = 25 µm. (N) Quantification of cleaved caspase-3 signal intensity (O.D.) (N = 5/group). (O) Neurological Severity Score (NSS) across experimental groups. Box plots show median, interquartile range, and min–max values; each dot represents one animal. *p < 0.05, **p < 0.01, ***p < 0.001, ****p < 0.0001.

Supplementary Files

This is a list of supplementary files associated with this preprint. Click to download.

- SupplementalFigs.pdf
- WesternBlotMembranesNutarellietal.pdf